ChemComm

COMMUNICATION

View Article Online
View Journal | View Issue

Cite this: *Chem. Commun.*, 2024, **60**, 5431

Received 1st April 2024,
Accepted 22nd April 2024

DOI: 10.1039/d4cc01497a

rsc.li/chemcomm

Mechanistic variances in NO release: *ortho vs. meta* isomers of nitrophenol and nitroaniline†

Prahlad Roy Chowdhury, Monali Kawade and G. Naresh Patwari *

The NO release following 266 nm photolysis of *ortho* and *meta* isomers of nitrophenol and nitroaniline shows a bimodal translational energy distribution, wherein the slow and fast components originate from dynamics in the S_0 and T_1 states, respectively. The translational energy distribution profiles for any NO product state show a higher slow-to-fast (s/f) branching ratio for the *ortho* isomer in comparison with the *meta* isomer. The observed variation in the s/f branching ratio *vis-à-vis* the *ortho* and *meta* isomers is attributed to the presence of intramolecular hydrogen bonding between the *ortho* substituent and NO_2 moiety, which favours the roaming mechanism.

Nitroaromatic compounds produce nitric oxide (NO) upon irradiation, which modulates the oxidative capacity of the atmosphere.[1,2] Measurements on the translational energy distribution of NO fragments following UV photolysis of nitroaromatic compounds show the presence of slow and fast components (a bimodal behaviour), which has been interpreted as the presence of two distinct pathways for NO release.[3,4] The absence of a direct route to produce NO from nitroaromatic compounds suggests that both pathways must proceed *via* nitro-to-nitrite photoisomerization. The 266 nm excitation of nitrobenzene to high-lying electronic states (S_4/S_3) results in ultrafast relaxation to the T_1 state with a timescale of about 200 fs, and thereafter the dynamics on the T_1 surface is much slower with the lifetime of about 90 ps, wherein the nuclear dynamics will dominate.[5] These observations are in accordance with the hypothesis that the topography of the T_1 surface influences the dynamics of NO formation.[3] Based on electronic structure calculations, the fast NO component is attributed to a direct elimination channel from the T_1 state featuring an oxaziridine ring-type (tight) transition state.[3,4,6] On the other hand, the slow translational energy component of the NO radical is attributed to nitro-to-nitrite photoisomerization in the ground state, either arising from an oxaziridine ring-type and/or a NO_2 roaming transition state. The NO_2 roaming mechanism originates from the frustrated dissociation of the C–N bond in nitrobenzene and the NO_2 radical is trapped in a shallow potential well around the phenyl radical and "roams" to form phenyl nitrite (C_6H_5ONO), and the release of NO radical with low translational energy is attributed to the presence of an exit barrier for O–NO bond dissociation.[4] Thus far, it has been inferred that the slow translational energy component of the NO radical originates from the S_0 state with both roaming and non-roaming (oxaziridine ring-type) mechanisms. Recent high-level electronic structure calculations have suggested that the topography of the T_1/S_0 crossing points influences the slow and fast translational energy components of NO, which could involve oxaziridine or roaming-type geometries, and the roaming pathway has a relatively higher (4.61 eV) barrier.[7]

The ability of T_1 surface topography to direct the NO release *via* the oxaziridine or roaming-type mechanisms, and thereby influence the relative yields of the fast and slow translational energy components, was investigated in several *ortho*-substituted nitrobenzenes by probing a specific NO fragment ($v = 1$; $J = 50.5$) state.[8] In these cases the appearance of the bimodal translation energy distribution profile of the NO radical was dependent on the nature of the substituent. The substituents that were capable of forming intramolecular hydrogen bonding with the NO_2 group, such as OH and NH_2 groups, favoured the slow component over the fast component. In other words, the slow-to-fast (s/f) branching ratio between the components of the total translation energy distribution profile of NO was greater than one (s/f $>$ 1) in the case of *o*-nitrophenol and *o*-nitroaniline. On the other hand, a reverse trend with s/f $<$ 1 was observed for *o*-nitroanisole and *o*-nitrotoluene, wherein the substituents do not hydrogen bond with NO_2. The experimentally observed results were interpreted on the basis of two-dimensional potential energy surfaces (2D-PESs) in the T_1 state and it was inferred that the minimum energy path favours the NO_2 roaming mechanism for the

Department of Chemistry, Indian Institute of Technology Bombay, Powai, Mumbai 400076, India. E-mail: naresh@chem.iitb.ac.in

† Electronic supplementary information (ESI) available: Methodology, 2D-PES at the M0-62X/6-311++G (d,p) level, one dimensional cut of the T_1-2D-PES along the MEP of NO release, VMI images and fitting of the $[P(E_T)]$ profiles, and T_1/S_0 crossing in nitroaniline. See DOI: https://doi.org/10.1039/d4cc01497a

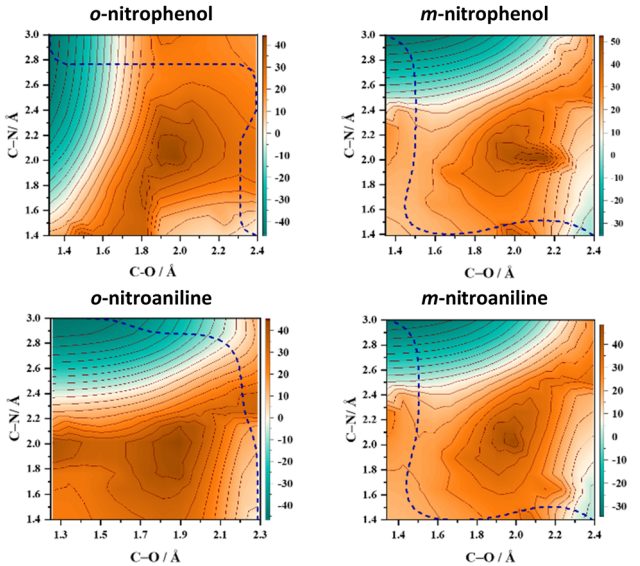

Fig. 1 Two-dimensional potential energy surface (2D-PES) plots of *o*-nitrophenol, *m*-nitrophenol, *o*-nitroaniline, and *m*-nitroaniline calculated using the B3LYP/6-311++G(d,p) level of theory. The blue dashed lines represent the minimum energy paths (MEPs) connecting the starting structure (bottom right corner) with the formation of NO and the co-fragment phenoxy radical (top left corner) in the T_1 state. The energy scale is in kcal mol^{-1} relative to the starting geometry on the T_1 surface. The one-dimensional cut of the 2D-PES along the minimum energy path resulting in NO release is shown in Fig. S1 (ESI†) along with the selected geometries.

substituents, in the *ortho* position, capable of hydrogen bonding (OH and NH_2), while in the other cases (H, CH_3, OCH_3 and CF_3 groups), the NO release *via* an oxaziridine ring-type mechanism is preferred.[8] On the other hand, the variation in the substituents at the *para* position had only a marginal influence on the s/f branching ratio.[9]

A pertinent question that arises at this state is: does the intramolecular hydrogen bonding between the NO_2 and the *ortho* substituent influence the NO release mechanism? To test this hypothesis 2D-PESs in the T_1 state were calculated for two pairs of substituted nitrobenzenes in which the OH and NH_2 groups were switched from the *ortho* position to the *meta* position and the corresponding 2D-PESs in the T_1 state are shown in Fig. 1 and Fig. S2 (ESI†). These 2D-PESs clearly illustrate that the minimum energy path switches from the NO_2 roaming mechanism to the oxaziridine ring-type mechanism for both OH and NH_2 substituents when shifted from the *ortho* to *meta* position, respectively. The topographical aspects of the 2D-PESs remained unaltered with two distinct DFT functionals *viz.*, B3LYP and M06-2X (compare Fig. 1 and Fig. S2, ESI†). Since the 2D-PES is the projection of the multi-dimensional potential on two nascent internal coordinates leading to NO release, it can be therefore hypothesised based on the minimum energy pathway in the 2D-PESs that the s/f ratio will be higher in the *ortho* isomer in comparison with the *meta* isomer.[8]

The experimental realization of this conjecture based on the 2D-PES calculation was carried out by measuring the total

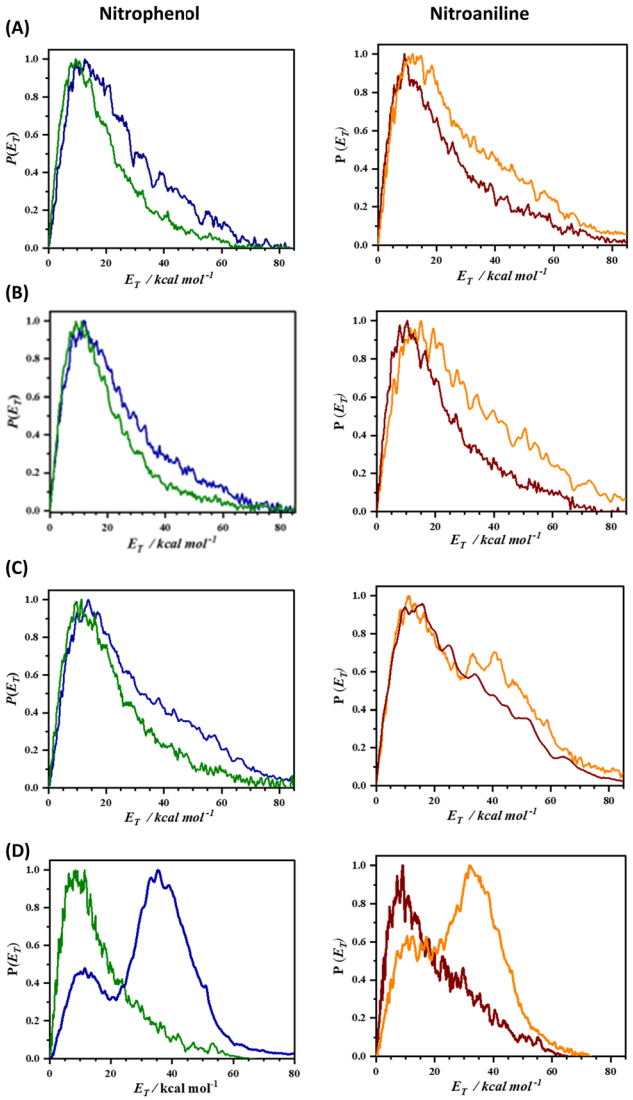

Fig. 2 The total translational energy distribution profiles [$P(E_T)$] of NO, produced from nitrophenol (left panel) and nitroaniline (right panel), probed for various product states of NO (A) v = 0; J = 21.5, (B) v = 0; J = 29.5, (C) v = 0; J = 33.5 and (D) v = 1; J = 50.5. The [$P(E_T)$] profiles of the *ortho* and *meta* nitrophenols are depicted by solid green and blue curves, respectively, while *ortho* and *meta* nitroanilines are represented by solid brown and orange curves, respectively. It is noteworthy that the fast component in the [$P(E_T)$] profiles of *meta* isomers is consistently higher than that of the *ortho* isomer across all the product states.

translational energy distribution profiles of NO produced from *o*-nitrophenol, *m*-nitrophenol, *o*-nitroaniline, and *m*-nitroaniline using the velocity map imaging (VMI) technique[10] and the results are presented in Fig. 2. In all the four NO product states that were probed, the translational energy distribution profiles show bimodal behaviour (see Fig. S3 and S4, ESI†) with the s/f branching ratio for the *ortho* isomer higher than the corresponding *meta* isomer (see Table 1). Additionally, the s/f ratio of *o*-nitrophenol is always higher than the *o*-nitroaniline, which is in accordance with the fact that the OH group forms stronger hydrogen bonds than the NH_2 group. These observations clearly reinforce the role of intramolecular hydrogen bonding in

Table 1 Slow-to-fast (s/f) branching ratios for various NO product states

	Nitrophenol		Nitroaniline	
NO product state	*ortho*	*meta*	*ortho*	*meta*
$v = 0; J = 21.5$	4.92	3.17	3.23	2.28
$v = 0; J = 29.5$	5.40	3.78	3.67	2.38
$v = 0; J = 33.5$	4.31	2.31	2.05	1.21
$v = 1; J = 50.5$	3.85	0.33	1.92	0.45

favouring the slow component. In general, the contribution from the fast component increases with rotational quantum number J, in agreement with the earlier reports;[4] however, this effect appears to be more prominent with an increase in vibrational quantum number v. It must be noted that the 2D-PES is a projection of the multidimensional potential in two-dimensions and hence a simplified model. The trends in the s/f branching ratio, therefore, are an indicator of the influence of the substituent to form intramolecular hydrogen bonding with the NO_2 group resulting in the enhancement of the roaming mechanism, thereby validating the initial hypothesis.

The topology of the T_1 surface regulates the preferential mechanism; however, it has been well established that the nature of the T_1/S_0 crossing points and the exit barrier on the S_0 surface dictate the translational energy of the NO products.[4,5,11–14] In order to assess the role of the S_0 surface on the translational energy distribution of the NO products, 2D-PESs in the S_0 state were also computed, which are depicted in Fig. 3 (and Fig. S5, ESI†). In the case of *o*-nitrophenol, an early (closer to the reactant) T_1/S_0 crossing point along the minimum energy path on the T_1 surface is a loose transition state, reflecting the NO_2 roaming mechanism. The NO_2 roaming and the oxaziridine mechanism are distinguished by evaluating the difference between the two N–O bonds, which is depicted in Fig. S6 (ESI†). The roaming path is characterized by a sudden and late change in the difference between two N–O bonds, whereas the oxaziridine pathway is more gradual. On the S_0 2D-PES, the pathway for NO release is corrugated with an exit barrier of about 14 kcal mol^{-1} (see Fig. 3) and the presence of several phenyl nitrite like intermediates, which ultimately result in slow NO release. Conversely, in the case of *m*-nitrophenol, a late (closer to the products) T_1/S_0 crossing point was observed along the minimum energy path on the T_1 surface, which leads to the fast translational energy component. The slow translational energy component of the NO release is generally attributed to the dynamics on the S_0 surface, which once again originates from the roaming and non-roaming mechanisms. Therefore, based on the present set of results, it can be inferred that intramolecular hydrogen bonding between the NO_2 and the substituent in the *ortho* position plays a pivotal role in enhancing the roaming mechanism, thereby resulting in a higher s/f ratio for the *ortho* isomer relative to the *meta* isomer as well as higher s/f ratio for the *o*-nitrophenol in comparison with *o*-nitroaniline.

Summarising, the branching ratio of the slow-to-fast (s/f) translational energy components, for various NO product states, shows a higher value for the *ortho* isomer in comparison to the *meta* isomer. Furthermore, consistently higher s/f ratio

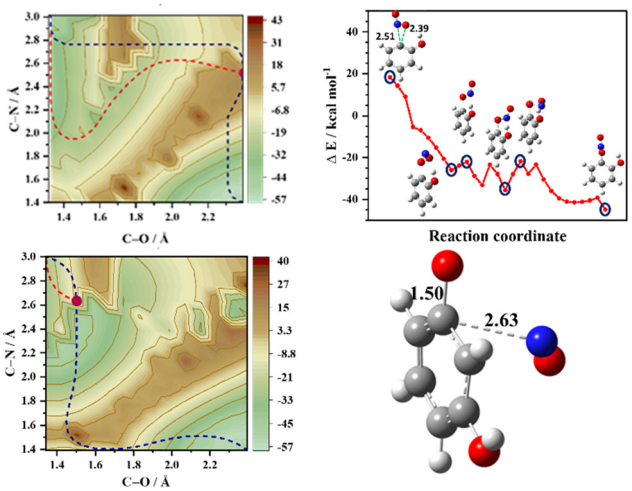

Fig. 3 Ground state (S_0) 2D-PES plots of *o*-nitrophenol (top left) and *m*-nitrophenol (bottom left) with the projected minimum energy path (MEP) that connects the reactant (bottom right corner) to the NO and phenoxy radical as products (top left corner) in the T_1 state (blue dashed line). The purple dot represents the T_1/S_0 crossing point along the T_1 MEP and the red dashed lines represent the MEPs in the S_0 state. Note that the T_1/S_0 crossing for *o*-nitrophenol and *m*-nitrophenol is early and late relative to the reactant, respectively. The S_0-MEP and selected structures after the T_1/S_0 crossing point for *o*-nitrophenol are shown (top right) along with the T_1/S_0 crossing point of *m*-nitrophenol (bottom right). The distances are shown in Å and the energy scale is in kcal mol^{-1} relative to the starting geometry in the T_1 state.

for the *o*-nitrophenol over *o*-nitroaniline is attributed to the OH group's propensity to form stronger hydrogen bonds compared to the NH_2 group. Therefore, it is inferred that the *ortho* isomer preferentially releases the slower NO fragments, which is attributed to the minimum energy roaming path. On the other hand, in the *meta* isomers, the faster component mediated *via* the oxaziridine pathway is enhanced. Thus, it has been illustrated that the hydrogen bonding ability of the substituent in the *ortho* position to the NO_2 group favours the roaming mechanism.

A skimmed molecular beam of helium doped with the heated (330–350 K) reagents (*o*-nitrophenol, *m*-nitrophenol, *o*-nitroaniline, and *m*-nitroaniline; Sigma Aldrich) was intersected by a counter-propagating pump (266 nm) and probe lasers[15] and the ensuing NO cations were detected *via* the $A^2\Pi - (X^2\Pi)$ [(0,0); Q_1 ($J = 21.5$; 29.5; 33.5)] and $A^2\Pi - (X^2\Pi)$ [(1,0); P_1 $J = 50.5$][16,17] and imaged. Each image was collected for 50 000 shots, which were symmetrized using ImageJ software.[18] Abel inversion was carried out by the Basis Set Expansion method (BASEX) to extract the translational energy distribution.[19] The plane of polarization of both lasers is kept parallel to the plane of the detector and the laser flux was optimized such that the signal intensity for the NO fragment was observed only in the presence of both the pump and probe lasers. The total translational energy profiles [$P(E_T)$], black traces in Fig. S3 and S4 (ESI†), were fitted to a bimodal empirical function,[8,20,21]

$$P(E_T) = C\cdot[(E_T)^{a_1}\cdot(E_T^{max} - E_T)^{b_1} + (E_T)^{a_2}\cdot(E_T^{max} - E_T)^{b_2}]$$

where a_1, a_2, b_1, and b_2 are adjustable parameters, C is a normalization constant, and E_T^{max} is the maximum total

translational kinetic energy available for the fragments in the centre-of-mass frame after dissociation.

The experimental results were interpreted by calculating the two-dimensional potential energy surfaces (2D-PES) in the ground (S_0) and first excited triplet (T_1) states with the B3LYP/6-311++G(d,p) and M06-2X/6-311++G(d,p) levels of theory using the Gaussian 09 suite of programs.[22] The 2D-PESs were mapped along two internal coordinates; the C–N bond ("C" referring to the carbon atom of the aromatic ring to which the nitrogen atom "N" of the nitro group is attached) and C–O bond ("O" referring to the oxygen atom of the nitro group that is away from the *ortho* substitution, which later forms a bond with the "C" atom of the aromatic ring leading to NO release). The distances $R_{(C–N)}$ and $R_{(C–O)}$ are varied in the range 1.4 to 3.0 Å and 1.25 to 2.3 Å, respectively, in 14 equidistant steps on each coordinate resulting in 196 data points. The minimum energy path on the 2D-PES for the release of NO from each of the substituted nitrobenzenes was evaluated using the Minimum Energy Path Surface Analysis (MEPSA) tool.[23]

PRC thanks PMRF for the research fellowship and MK is supported by the Women Scientists Scheme of the Department of Science and Technology (Grant no. SR/WOS-A/CS-18/2019). Financial support from the Science and Engineering Research Board of the Department of Science and Technology (Grant no. CRG/2022/005470) and the Board of Research in Nuclear Sciences (BRNS Grant no. 58/14/18/2020) is gratefully acknowledged. The authors wish to thank Ms Shaivi Kesari and Ms Bhawana for their help in carrying out some of the experiments. GNP wishes to thank Kaleidoscope-2023 for stimulating discussions.

Conflicts of interest

The authors declare no conflict of interest.

Notes and references

1 E. G. Alvarez, D. Amedro, C. Afif, S. Gligorovski, C. Schoemacker, C. Fittschen, J. F. Doussin and H. Wortham, *Proc. Natl. Acad. Sci. U. S. A.*, 2013, **110**, 13294–13299.
2 G. Lammel and J. N. Cape, *Chem. Soc. Rev.*, 1996, **25**, 361–369.
3 M. F. Lin, Y. T. Lee, C. K. Ni, S. Xu and M. C. Lin, *J. Chem. Phys.*, 2007, **126**, 064310.
4 M. L. Hause, N. Herath, R. Zhu, M. C. Lin and A. G. Suits, *Nat. Chem.*, 2011, **3**, 932–937.
5 L. Saalbach, N. Kotsina, S. W. Crane, M. J. Paterson and D. Townsend, *J. Phys. Chem. A*, 2021, **125**, 7174–7184.
6 Y. He, A. Gahlmann, J. S. Feenstra, S. T. Park and A. H. Zewail, *Chem. – Asian J.*, 2006, **1**, 56–63.
7 A. Giussani and G. A. Worth, *J. Phys. Chem. Lett.*, 2024, **15**, 2216–2221.
8 N. B. Bejoy, P. Roy Chowdhury and G. N. Patwari, *J. Phys. Chem. Lett.*, 2023, **14**, 2816–2822.
9 N. B. Bejoy and G. N. Patwari, *J. Phys. Chem. A*, 2023, **127**, 7168–7169.
10 S. Mishra, N. B. Bejoy, M. Kawade, H. P. Upadhyaya and G. N. Patwari, *J. Chem. Sci.*, 2021, **133**, 128.
11 A. Giussani and G. A. Worth, *J. Chem. Theory Comput.*, 2017, **13**, 2777–2788.
12 J. Mewes, V. Jovanovic, C. M. Marian and A. Dreuw, *Phys. Chem. Chem. Phys.*, 2014, 12393–12406.
13 H. A. Ernst, T. J. A. Wolf, O. Schalk, N. González-García, A. E. Boguslavskiy, A. Stolow, M. Olzmann and A. N. Unterreiner, *J. Phys. Chem. A*, 2015, **119**, 9225–9235.
14 A. Giussani and G. A. Worth, *Phys. Chem. Chem. Phys.*, 2020, **22**, 15945–15952.
15 S. Singh, M. Kawade, P. R. Chowdhury and G. N. Patwari, *J. Chem. Sci.*, 2023, **135**, 1–10.
16 R. P. E. Engleman Jr, H. M. Peek and V. D. Baiamonte, 1970, DOI: **10.2172/4128104**.
17 M. Sumida, Y. Kohge, K. Yamasaki and H. Kohguchi, *J. Chem. Phys.*, 2016, **144**, 64304–64312.
18 C. A. Schneider, W. S. Rasband and K. W. Eliceiri, *Nat. Methods*, 2012, **9**, 671–675.
19 S. M. Poullain, D. V. Chicharro, L. Rubio-Lago, A. García-Vela and L. Bañares, *Philos. Trans. R. Soc., A*, 2017, **375**, 20160205.
20 C. T. Matthaei, D. P. Mukhopadhyay and I. Fischer, *J. Phys. Chem. A*, 2021, **125**, 2816–2825.
21 H. J. Deyerl, I. Fischer and P. Chen, *J. Chem. Phys.*, 1999, **111**, 3441–3448.
22 M. J. Frisch, G. W. Trucks, H. B. Schlegel, G. E. Scuseria, M. A. Robb, J. R. Cheeseman, G. Scalmani, V. Barone, B. Mennucci, G. A. Petersson, H. Nakatsuji, M. Caricato, X. Li, H. P. Hratchian, A. F. Izmaylov, J. Bloino, G. Zheng, J. L. Sonnenberg, M. Hada, M. Ehara, K. Toyota, R. Fukuda, J. Hasegawa, M. Ishida, T. Nakajima, Y. Honda, O. Kitao, H. Nakai, T. Vreven, J. A. Montgomery Jr., J. E. Peralta, F. Ogliaro, M. Bearpark, J. J. Heyd, E. Brothers, K. N. Kudin, V. N. Staroverov, R. Kobayashi, J. Normand, K. Raghavachari, A. Rendell, J. C. Burant, S. S. Iyengar, J. Tomasi, M. Cossi, N. Rega, J. M. Millam, M. Klene, J. E. Knox, J. B. Cross, V. Bakken, C. Adamo, J. Jaramillo, R. Gomperts, R. E. Stratmann, O. Yazyev, A. J. Austin, R. Cammi, C. Pomelli, J. W. Ochterski, R. L. Martin, K. Morokuma, V. G. Zakrzewski, G. A. Voth, P. Salvador, J. J. Dannenberg, S. Dapprich, A. D. Daniels, Ö. Farkas, J. B. Foresman, J. V. Ortiz, J. Cioslowski and D. J. Fox, *Gaussian 09, Revision D.01*, Gaussian Inc., Wallingford CT, 2009.
23 I. Marcos-Alcalde, J. Setoain, J. I. Mendieta-Moreno, J. Mendieta and P. Gómez-Puertas, *Bioinformatics*, 2015, **31**, 3853–3855.

